Smart Structures and Systems, *Vol. 27, No. 6 (2021) 927-942*
DOI: https://doi.org/10.12989/sss.2021.27.6.927

Push-over bending and shear behavior assessments of hidden boundary void precast concrete slab with bi-tensional prestress

Phan Anh Nguyen [1a], Jeonghoi Kim [2], Jonghwan Oh [2], Youngshik Park [2], Sejung Lee [3] and Dongkyu Lee*[1]

[1] *Department of Architectural Engineering, Sejong University, Seoul 05006, Republic of Korea*
[2] *Technical Research Institute, IS Dongseo, Seoul 06071, Republic of Korea*
[3] *Sejin R&S, Seoul, Republic of Korea*

(*Received August 20, 2019, Revised February 1, 2021, Accepted February 18, 2021*)

Abstract. This paper presents a first proposed real-sized Hidden boundary Void precast concrete Slab, a so-called HVS. In order to assess and investigate push-over behaviors of the novel structural system, five types of real size specimens manufactured in factory are tested by corresponding static loading protocol experiments. Bending tests along with shear tests in both cases of presence and absence of topping concrete slabs are performed. Besides, composite slabs, which are two half-unit products connected by steel plates and U-bolts in the long edges, are surveyed to assess uniform characteristics of slab systems. Simultaneously, estimating calculations are proposed for the structural bearing capacity of partially prestressed concrete flagged sections. Proposed equations are developed according to provisions of several current global and local design standards. Moreover, this study provides another predicting approach using finite element analysis of MIDAS FEA for analytical performances of specimens. Thanks to these experimental and analytical results, the general characteristic of HVS may be observed, and then studied for realization in the field of prestressed precast concrete industries for construction.

Keywords: hidden boundary; void slab; HVS; precast slab; bi-tensional prestress; push-over static behavior; finite element analysis; bending test; sheear test

1. Introduction

For a long time, designers and manufacturers of building floor systems have tried to reduce the weight of slabs, while resistance performances required by structures are also satisfied. Among a variety of production techniques, creating appropriate voids or non-material regions is an effective and common practice. Conventional void slab and forming systems include waffle slabs (Guo *et al*. 2017), single- and double-direction span formwork systems (Yang *et al*. 2016, Park *et al*. 2009) together with hollow-core slabs (Nguyen *et al*. 2019, Li *et al*. 2018a, b). There are also some recent developing systems such as bubble deck (Shetkarand and Hanche 2015), cobiax, EPS slab, u-boot, bee plate and air deck (Churakov 2014). Void slabs may reduce costs for building and bridge constructions by saving materials. Indeed, voided slabs eliminate concrete materials which are not needed for resisting structural performance. The subsequent weight reduction gives the opportunity to make longer spans up to about 15m between two columns without beams as well as allows lighter foundations (Amadeo *et al*. 2018). Moreover, voided slabs may be beneficial in seismic designs (Kim *et al*. 2012), since the reduced dead weight of floors results in lower load effects applied to structures insipred by lower resistances. Slabs with voids filled by air (thermal conductivity = 0.025 W/mK) are efficient with respect to the insulation and reduction of noises (Paik and Na 2018). Optimization concepts (Lee *et al*. 2017, 2018, Lee and Banh 2018) and reinforced methods with nanofiber (Motezaker and Kolahchi 2017, Motezaker and Eyvazian 2020a, b) may be utilized in advance for increasing structural performances and reducing materials, even if they are not treated in this study.

Recently, void slabs with prestressed wires have been ubiquitously applied to various structures such as stores, warehouses, stadiums and other spatial structures. In this paper, a newly developed void precast wire-prestressed concrete slab - HVS, consisting of an inverted rib slab (Lee and Park 2010) together with a topping concrete component, is proposed for general parking buildings (Zuo *et al*. 2010). While the inverted rib slab is a precast member, the topping concrete is a cast-in-site element; therefore, in this study, they are named as PC (precast concrete) and RC (reinforced concrete) slab, respectively. There is a minutia of shapes but it plays core function creating advantages of HVS. 18mm-concave corners are molded on both sides of ribs in the precast period. On construction sites, concave corners hold thin plates of timber which play roles of bottom formworks for topping concrete as well as locking empty parts to create voids.

In comparison with conventional void slabs, HVS needs not additional reinforcements to prevent a buoyancy of the

*Corresponding author, Associate Professor,
E-mail: dongkyulee@sejong.ac.kr
[a] Master Student, E-mail: phananhxdbk1993@gmail.com

ISSN: 1738-1584 (Print), 1738-1991 (Online)

landfill when casting concrete (Marais *et al*. 2010), that helps the manufacturing process, is much faster, easier and less labor requested. In this case, the application of the thin timber for HVS is superior to other kinds such as bubble, u-boot, and cobiax when it is not only economical and flexible in adjusting but also convenient to on-site store and transfer.

In the precast concrete structure, contiguous regions or boundaries of PC members are the most essential and sensitive areas. The structural response will depend on the behavior and the characteristics of the connections (Björn 2008). With HVS, the present topping concrete part aims to not only reinforce the precast member but also make the surface smooth and prevent material leaks near at continuation areas of PC slabs. It is the reason why "hidden boundary" is mentioned in this slab system. Besides, upward cambers, often occurring by prestressed units, do not have identical heights and angles among all slabs. Consequently, erratic upper surfaces may lead to reduce the quality of topping concrete in terms of reinforcement-cover, and bottom surfaces may take defects at contiguous areas, as well. To minimize the camber disparities among PC members, proposing shear connectors not only link PC members as usual methods, but they also an adjust camber's value using a hand machine. In practice, the adjusted cambers from 7mm to 10mm are recorded. Not only provides a proposed calculation of design thickness of shear connectors, but also investigates the design results in both test and analysis to assure the working ability in installation.

This study presents experimental results for assessing structural responses such as flexural and shear strengths of slabs. Simultaneously, to get theoretical results as a reference before the test, several global and local standards such as ACI 318, EN: Eurocode 2, PCI, AASHTO 2002, KCI 2012 and CSA A.23 are considered to propose the bearing capacity and the deflection of the specimens. In

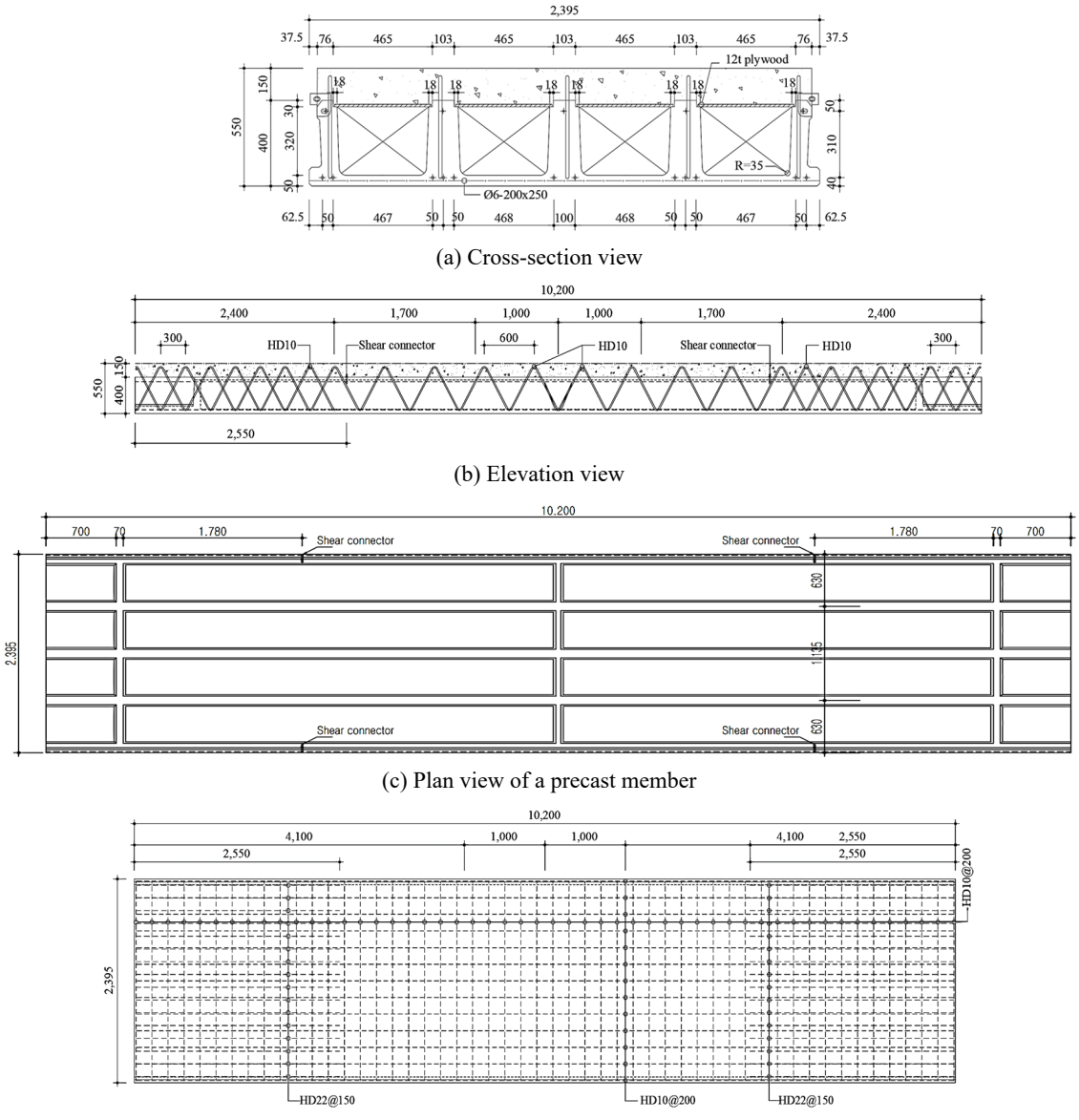

Fig. 1 Details of the HVS product

comparison with the experimental result, finite element analysis of commercial MIDAS FEA software provides stable iterative calculation methods for solving nonlinear equations and their respective options.

The organization of this paper is listed as follows. Details of HVS begin in Section 2 with an overall structure and manufacturing process. In Section 3, a brief description of formulations and prediction procedures for bending and shear design along with the analytical method in MIDAS FEA are presented. Section 4 describes experimental objectives. Results of theorical predictions, finite element analysis as well as experiments are shown in Section 5. Conclusions are drawn in Section 6. And then, an Appendix is shown for theoretical backgrounds of the proposed prediction calculation.

2. Description of Hidden boundary Void precast concrete Slab- HVS

2.1 Overall structure

The HVS product has 10.2m in length and 2.4m in width as shown in Fig. 1. The height of the PC part is 400 mm, while the thickness of the topping part is 150mm. Five inverted ribs are placed on the PC member, which creates four trapezoidal hollows at equal intervals. That help HVS save up to 46% material compared to solid slabs.

To introduce a prestress, a seven-wire Φ9.5 strand is installed at the upper part of each rib. Simultaneously, in lower parts of ribs, total twelve seven-wire Φ15.2 strands are set. Particularly, while the center and two fringe ribs also have two strands, there are three steel wires in the other ribs. Φ6-200-200 wire mesh is installed in the lower flange to prevent cracks due to the temperature along with drying shrinkage. As shown in Figs. 1(a)-(b), HVS is manipulated by a lattice-type with HD10 in the rib, instead of the usual loop reinforcement type, to secure against the shear force. Especially, regions at about 2400mm of both ends receive most of the shear impact in a slab, and then double V-bars are set up. Moreover, top parts of V-bars protruding from the PC unit are attached to reinforce in topping concrete. It has HVS become a composite structure.

Topping reinforcement is shown in Fig. 1(d). The HD10-200×200 wire mesh plays a role of linking with PC members and the support for flexural performance. Besides, HD22 reinforcing bars are arranged at 150mm intervals at both ends of topping parts to enhance bearing capacity of the negative moment at slab-column conjunction. To easily observe how HVS is fabricated, Fig. 2 illustrates the manufacturing process on factory. This process is not only to fabricate specimens in this study but also the same manner to make the real HVS products including the precast and cast for the actual application. Input data of Table 1 is applied for the behavior calculation process in Section 3.

2.2 Shear connector

As a specific characteristic of HVS and, a shear connector is shown in Fig. 3. It consists of steel plates and U-bolts, which are developed to link PC members and fasten them during construction period on factory until casting the topping concrete. Moreover, this kind of shear

Table 1 Material properties

Material		Properties (MPa)	
Concrete	f_c'	45	PC compression strength
	f_{ct}'	25	Topping compression strength
Rebar	f_y	400	Tensile strength of rebar
Top strand (7 wires Ø15.2mm)	f_{pu}	1.860	Tensile strength of strand
	f_{py}	1.590	Yield strength
	A_p	138.7	Cross-sectional area (mm^2)
Bottom strand (7 wires Ø9.5mm)	f_{pu}	1.860	Tensile strength of strand
	f_{py}	1.674	Yield strength
	A_p	54.84	Cross-sectional area (mm^2)

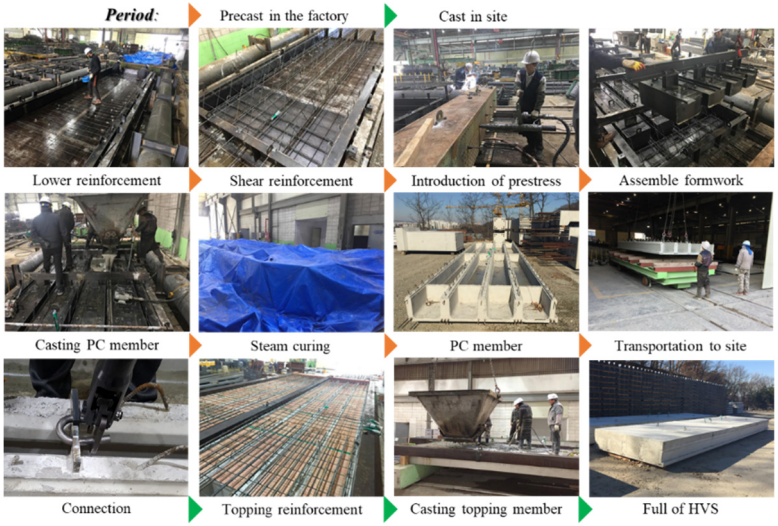

Fig. 2 Factory manufacturing processes of a HVS specimen

connector is expected to minimize the difference of a camber that usually occurs in PC units while prestressed. Particularly, in the period of installation as shown in Fig. 2, the steel plates balance the elevation by the machine before being locked by U-bolt. Usually, an allowable error of the difference in height of PC members is within around 20mm according to actual camber values recorded in the factory. In order to adjust the camber of slabs evenly, two steel plates are placed at 1/4 of total length of the members from each ends.

This study proposes the calculations to obtain the essential thickness for the shear connector. Actually, this component is not available in terms of design standards; therefore, the proposed guideline is based on real behavior. As can be seen, a steel plate has two holes to include an upper hole connected with the U-bolt and a lower hole attached to a transverse rebar or strand. Therefore, the design problem is that shear connectors have to be stable under the force to balance difference deflection from the prestressed period. This paper proposes requirements for the thickness of a connector through surveying four specific positions and during the construction time as shown in Fig. 4 and explained in details in Appendix.

To scrutinize the design results, finite element analysis for the shear connector is carried out by MIDAS FEA. According to the above design results, the thicknesses of a steel plate and the diameter of U-bolt are 15mm and 19mm, which are applied as input data of analyses. Materials of steel plates and U-bolt are identified by SS400 and SM45C whose yield stresses are 235MPa and 343MPa, respectively. This analysis aims to check bearing capacities of shear connectors and U-bolt under impacts from the machine to balance cambers between two PC members, as shown in Fig. 5(a). The load acts on shear connectors (Chahnasir *et al*. 2018, Sedghi *et al*. 2018) based on the camber difference of PC member. Fig. 4 presents the installation shear connector in the construction site.

In MIDAS FEA, steel plates are modelled as an auto-mesh by using 3D solid elements as shown in Fig. 6. Simultaneously, an elastic perfectly plastic model is used in

(a) Installation (b) Installed

Fig. 5 Practices of the shear connector

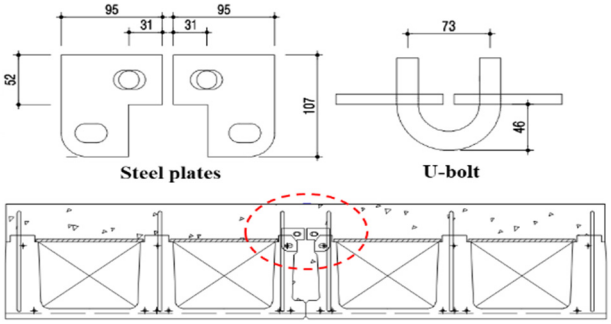

Fig. 3 Details of the shear connector

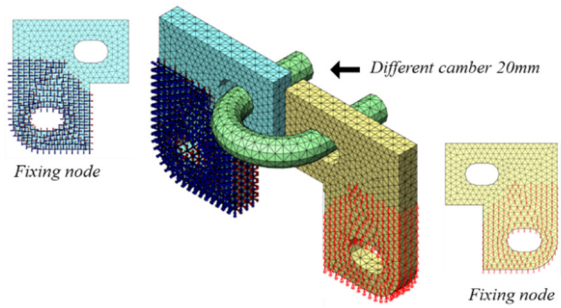

Fig. 6 Configuration of the shear connector

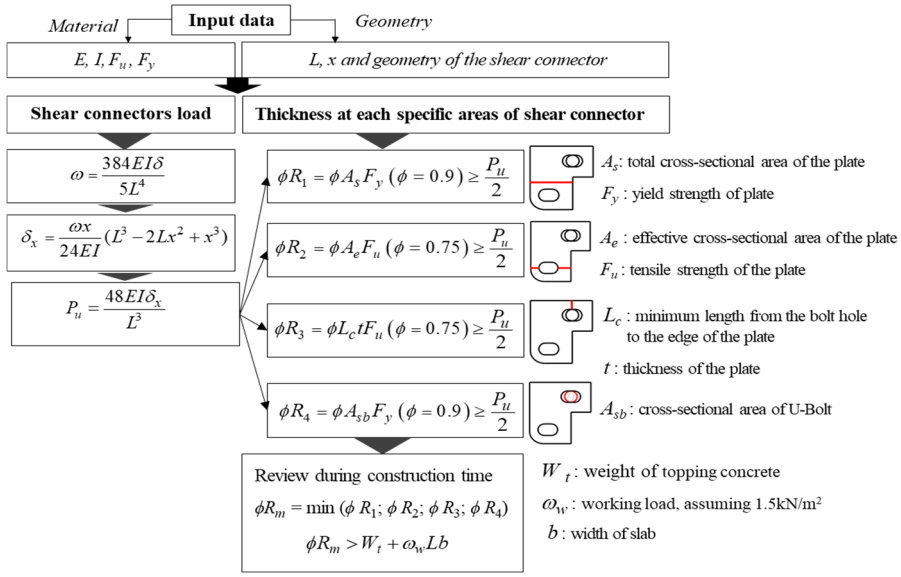

Fig. 4 Design procedures of shear connector's thickness

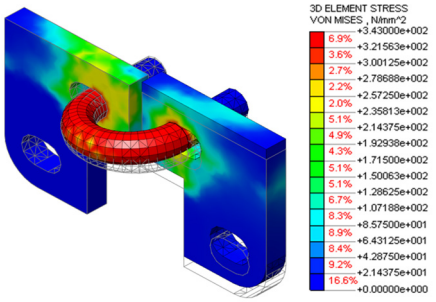

Fig. 7 Stress distribution of the shear connector

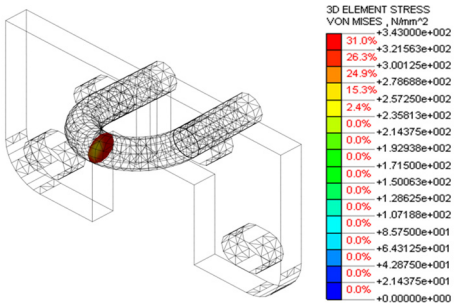

Fig. 8 Stress distribution of the U-bolt section

the analysis. In the time of installation, while upper parts of two steel plates receive the load P_u, as shown in Fig. 5, two lower parts are assumed to be embedded completely in PC member and free from the load. At the same time, deflections on steel plates lead to a torsion load on U-bolt.

Results of MIDAS FEA for shear connectors in the installation, especially Von-Mises stress distributions (Lesani *et al*. 2017), are shown in Fig. 7. The embedded parts of steel plates do not display any stress while upper parts receiving force show to be partially yielded at the interface with U-bolt. However, most of the sections are elastic state due to a local stress concentration. As shown in Fig. 8, U-bolt section yield by torsion indicates 31% of total cross-section.

About 70% of the cross section shows the elastic stress. Moreover, according to the actual status of the shear connectors in Fig. 5(b), there is not any damage after installing. Therefore, U-bolt and plate steels are stable against the displacement loads due to expected camber difference.

3. Basic bending and shear calculations and analyses

3.1 Flexural strength

This study considers several current global and local design standards such as ACI-318, PCI 2004, AASHTO 2002, KCI 2012 and CSA A.23 for prestressed concrete structures. Through comparisons and combinations among those codes, the proposed calculations of flexural strength of the general partially prestressed concrete flagged section are summarized in Fig. 9 as well as explained in details in Appendix.

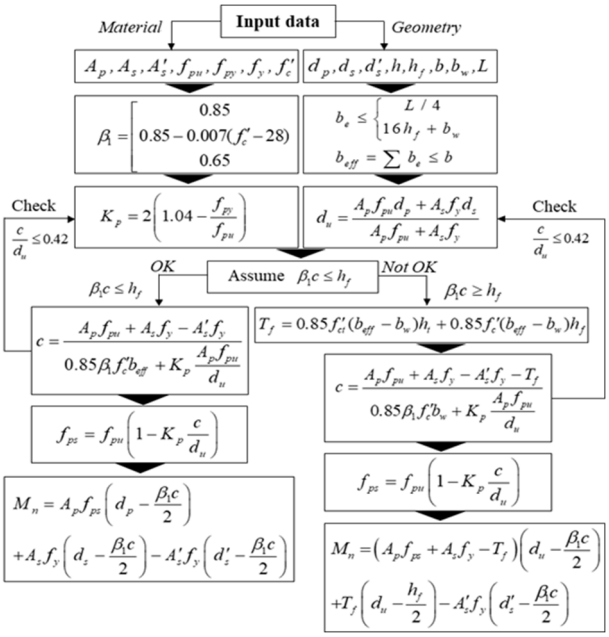

Fig. 9 Prediction procedures of the nominal flexural strength

3.2 Shear strength:

Nowadays, many models are available to predict the shear strength of prestressed concrete members. However, there is little consensus among codes as to which is the most accurate and suited for designs. As a result, there are several design specifications based on different models. This study provides the background of shear design methods to be contained in several current global design standards as ACI-318, AASHTO 2002 and local codes as KCI 2012, CSA A.23. After comparisons and combinations among those codes, a proposal prediction method is presented in Appendix and summarized in Fig. 10.

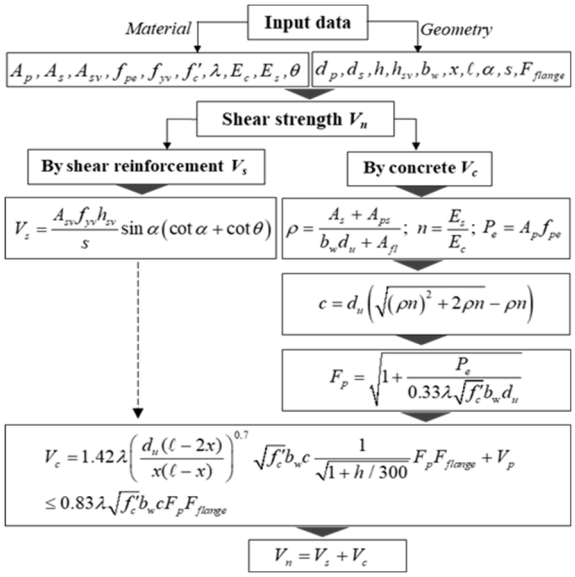

Fig. 10 Prediction procedures of the nominal shear strength

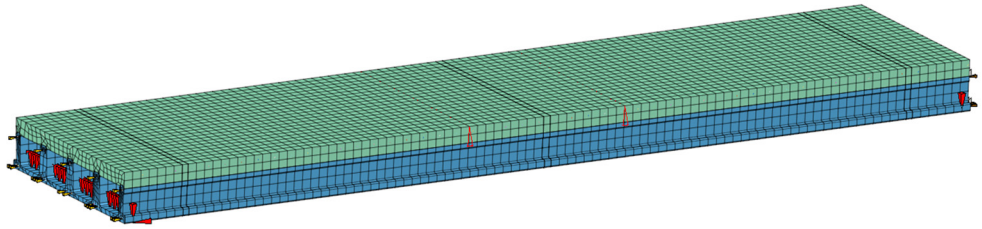

(a) PC member and topping concrete (3D solid element)

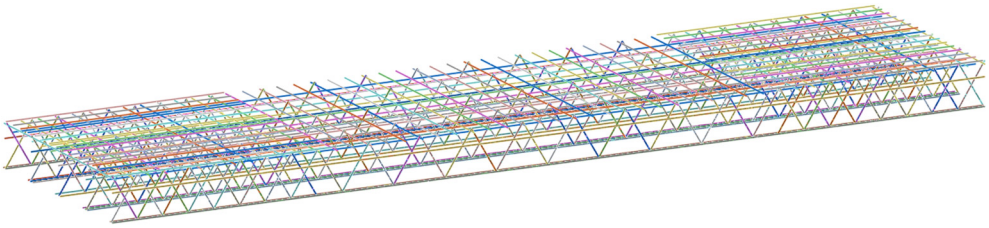

(b) Stiffeners and bars (bars in solid element)

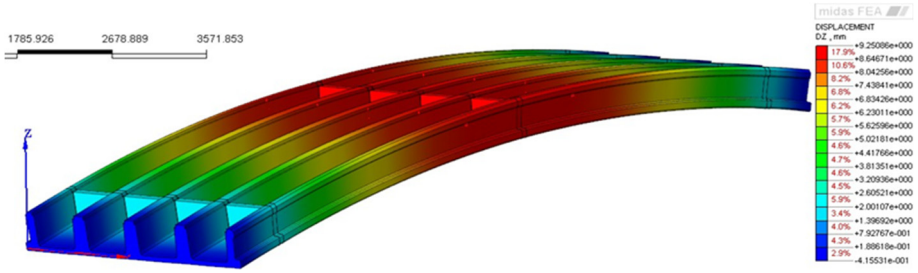

(c) Camber of the PC slab after prestressing

Fig. 11 Bending and shear models

3.3 Finite element model by MIDAS FEA

MIDAS FEA, combining a powerful pre/post processor and solver co-developed by MIDAS IT and TNO DIANA, stands for the reliability and accurate solutions and is founded on an expertise in geometry modeling, Auto-mesh generation, contemporary graphics and analysis technologies (Wu and Peng 2018). MIDAS FEA is equipped with advanced geometric modeling functions, powerful mesh generation algorithms, various analysis conditions and exceptional output displays with the latest graphics technology. The general work sequence of MIDAS FEA is as follows: Geometry Modeling, Mesh Generation, Analysis Condition, Analysis and Post-processing and Result Evaluation.

In order to investigate the behavior of slabs, each component such as geometrical shape, concrete, reinforcement and prestressed strand is modelled according to actual size and properties, as example of HVS shown in Fig. 11. For the kind of partially prestressed concrete structures as HVS, MIDAS FEA is an effective analyzing aid. Even, it is more convenient than other common software such as ABAQUS, ANSYS, SAP2000, ETABS. Indeed, while other softwares ignore or require several sub-simulations to analyze prestressed strands, parameters of the tendon are available in MIDAS. The value of tensile force, loading conditions and the manner of the prestressed period as camber-phenomenon, as shown in Fig. 11(c), can be applied to MIDAS. Moreover, analyses consider immediate loss (friction, slip and elastic deformation and long-term loss (tendon relaxation, creep/shrinkage effect)). Therefore, it can improve the reliability and shortened analysis time for modeling.

In an analysis step of MIDAS, boundary conditions and loading conditions are assigned according to real experiments. However, another significant task, which defines material properties, requires various parameters such as Elastic modulus, Poisson's ratio, shear modulus, weight density, expansion coefficient and so on. To simulate nonlinear behavior in this study, the total strain crack function is manipulated as shown in Fig. 12. The function type of Brittle in Fig. 12(b) is assigned for tension models like a reinforcement (Lee *et al*. 2015). Brittle behaviors are characterized by the full reduction of the strength after the strength criterion is violated. Simultaneously, a constitutive

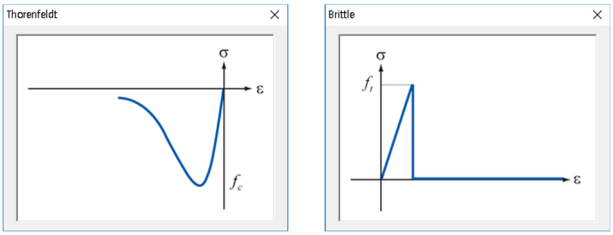

(a) Compressive stress-strain curve (b) Tensile stress-strain curve

Fig. 12 Tensile stress-strain curves

model for the concrete in compression suggested by Thorenfeldt *et al*. (1987) has been used to describe the compressive behavior of concrete in the direction of the principal compressive strain.

4. Experimental objectives

Five specimens of bending tests along with shear tests in both cases of presence and absence of topping concrete slabs are performed and based on their thickness. Types of experiments are shown in Table 2. This study not only confirms the bending performance of specimen M-400 and M-550, but also specimen CM-550 is made to survey the bending performance at the midpoint section of a composite slab that is two half-part slabs connected by steel plates and U-bolts in the long edges.

The experimental tests are carried out at a hybrid structural test laboratory. The force device is an actuator with a capacity of 3000kN and is driven by a displacement control method (Major 2012). The load force is measured using a load cell attached to the actuator as shown in Fig. 13.

Table 2 Specimen notations in tests

No.	Specimen	Type of experiment	Type of member	Remarks
1	M-400	Flexual test	PC only	
2	M-550		PC+Topping	
3	CM-550			Slab connection
4	S-400	Shear test	PC only	
5	S-550		PC+Topping	

Specimen notation:
Experimental thickness: PC part: 400 mm,
Composite slab: 550 mm
Type of experiment:
M : flexure by positive moment
CM : flexure by positive moment of specimen having connector
S : shear

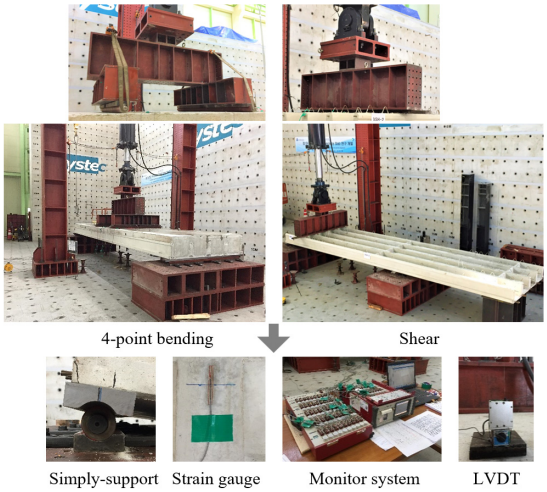

Fig. 13 Setting situation for the test

As an experimental method, the slab is put in the designed location, that is suitable for the loading and supporting system. All concrete and reinforcing gauges along with LVDT are connected to a monitor system to get the data. A given loading protocol condition is gradually set by 0.01, 0.03, 0.07 and 0.1mm/s until failure. In four-point bending test, the load has 2 points around the middle whose distance is 1900mm. The setting for shear test is that one of simple supports is set at a distance of 100mm from the end while the other is installed at a distance of 5000mm from loading points. Fig. 13 illustrates setting situations for both tests (Sovják *et al*. 2012).

5. Results and discussion

5.1 Bending test results of finite element analysis and experiment of M-400

The test specimens M-400 measures bending strength in the construction stage of the PC member before casting topping concrete. Fig. 14(a) presents the comparison of load-displacement curves of M-400 in real experiments as well as in analyses by MIDAS FEA and nominal bending moment M_n based on suggested equations in Section 3.

Before the initial crack, the load-displacement curve is linear to show elastic behavior of slab when load grows

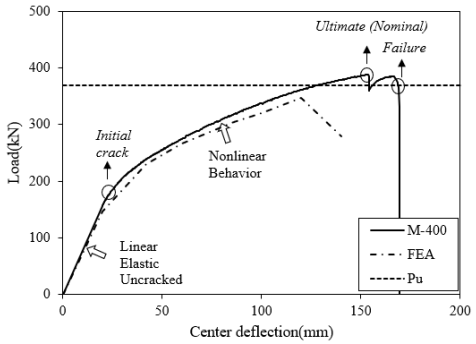

(a) Load-displacement curve of M-400 specimen

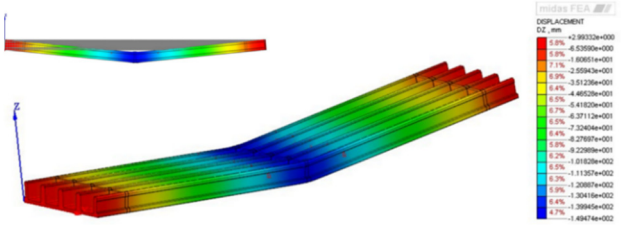

(b) Displacement contour in MIDAS FEA

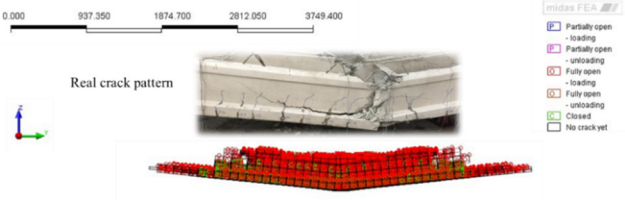

(c) Crack patterns in test and analysis of M-400

Fig. 14 Results of M-400

with small deflections. The initial bending fracture occurred at the center of the specimen which is recorded 168 kN of load and 22mm of deflections. Then, nonlinear behavior happens when displacement increases significantly along with a large number of flexural cracks which appear until reaching the nominal point at 388.84 kN. After that, the slab quickly collapsed as the usual brittle performance of a fully prestressed concrete component.

The estimated strength of proposed formulation is 369.7kN, which is 5% lower than the experimental result of 388.84kN. Besides, as a result of MIDAS analysis, the linear elastic uncracked period is nearly the same as experimental results. Then the nonlinear curve reaches a peak at 347.6kN and displacement of 120mm, as shown in Figs. 14(a)-(b). In general, analysis results by MIDAS FEA tend to be conservative with 10% lower than experimental data, but the flexural behavior is illustrated similarly to the test. Fig. 14(c) illustrates crack patterns taken from the nonlinear analysis in MIDAS in terms of an element status. It can reflect the real crack patterns in the experiment.

5.2 Bending test results of finite element analysis and experiment of M-550

In order to investigate bending performances of HVS, specimen M-550 is made by casting topping concrete on the PC member. Fig. 15(a) compares load-displacement curves of the specimen in an experiment along with the analysis and calculated nominal bending moment M_n. In general, the addition of topping concrete significantly improves both the bearing capacity and flexural behavior of HVS.

The load-displacement curve is linear elastic until the first crack occurs at 366kN and 17mm of the deflection. Before reaching the elastic limit, there is an almost linear portion (Linear Elastic Cracked), where the concrete is cracked. And both concrete and reinforcement can be considered in their linear elastic range of behaviors. The slope of this portion is smaller than that of the initial portion. A nonlinear region the response of the concrete is nonlinear and where gradual yielding of the reinforcement occurs. This region eventually leads to a maximum load of 706.7 kN. This value is about 8% higher than the prediction and analysis values of 649.36 kN and 640 kN, respectively. And in the real test, the topping concrete lets M-550 increase 45% of flexural capacity compared with M-400, from 388.84 kN to 706.7 kN.

Besides, the failure mode of M-550 is plasticity instead of brittle as M-400. Therefore, cracks widen extensively, giving warning before the concrete crushes and the structure collapses as shown in Fig. 15. Most design standards adopt this type of designs instead of the situation that the concrete fails suddenly, and the structure collapses immediately without any warning.

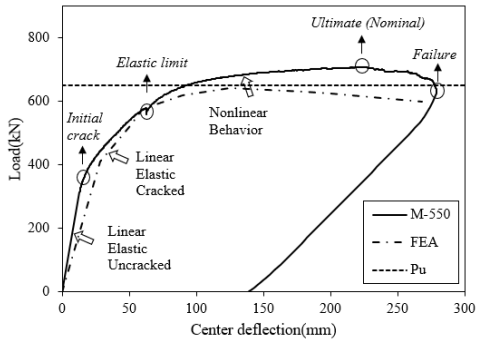

(a) Load-displacement curve of M-550

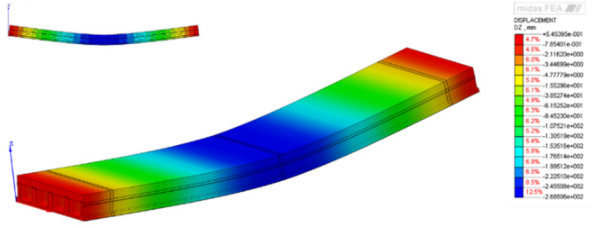

(b) Displacement contour in MIDAS FEA

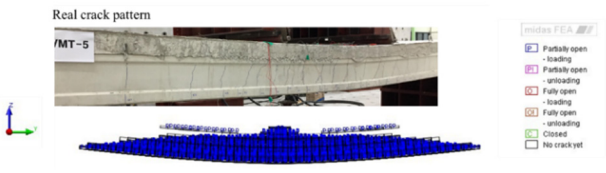

(c) Crack patterns in the test and analysis of VM-550

Fig. 15 Results of M-550

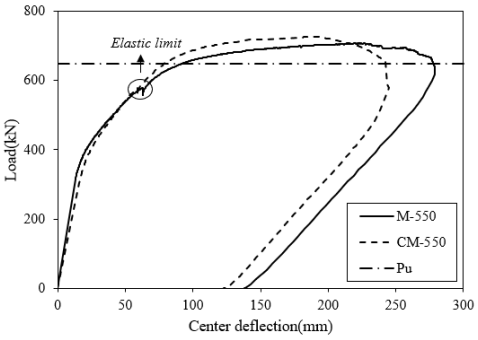

(a) Load-displacement curves of CM-550 and M-550

(b) Cracks of M-550

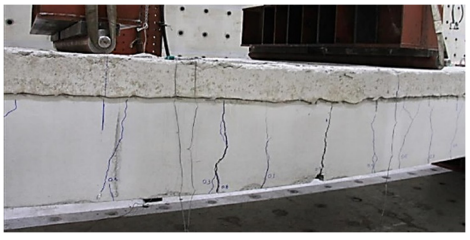

(c) Cracks of CM-550

Fig. 16 Results of CM-550 in comparison with M-550

5.3 Bending test results of finite element analysis and experiment of CM-550

Specimen CM-550 especially surveys the contiguous area of two units of PC members that contain shear connections as shown in Fig. 3. The experimental data is analyzed in comparisons with those of specimen M-550. According to Fig. 16(a), two kinds of slab obtain almost identical load-displacement curves in elastic portions. Despite slightly distinct in nonlinear portions, experimental results present a similar bending capacity and flexural behavior between CM-550 and M-550. It verifies the uniformity in performances of HVS, regardless of inner or adjacent areas of slabs.

As shown in Figs. 16(b)-(c), crack patterns of M-550 and CM-550 are similar with several cracks to develop around the middle of slab as the plastic mode of failures.

Besides, shear connectors are investigated in terms of deformation in which slabs suffer flexural load. Therefore, strain gauges are set up as in Fig. 17(a). The shear connector is attached by strain gauges at 16 positions and named as RC1-RC8 and LU1-LU8 for gauges on steel plates and U-bolt, respectively.

Deformations of shear connector in the bending test of specimen CM-550 are shown in Fig. 17. In general, the strain data at all positions is from -60×10^{-6} to 40×10^{-6}, which are lower than the normal yield strain (the strain corresponding to ultimate stress) of steel (0.2%). Shear connectors in HVS are stable when the slab receives the bending load. In other words, adjacent areas are not at a risk of dividing the system into discontinuous parts that could lead to common defects of a precast structure such as leakage and structural separation.

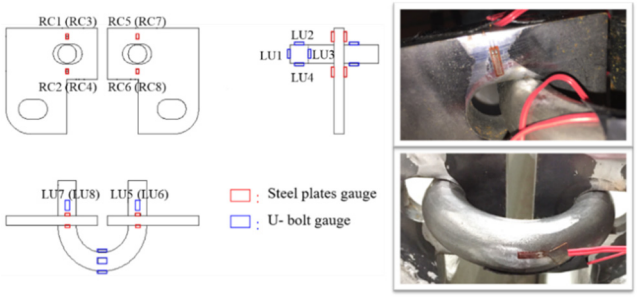

(a) Setting strain gauges for shear connectors

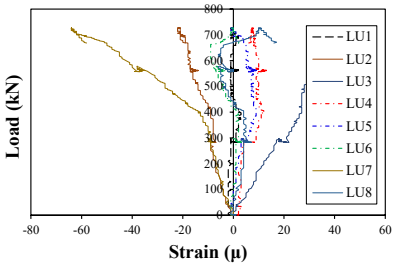

(b) U-bolt gauges

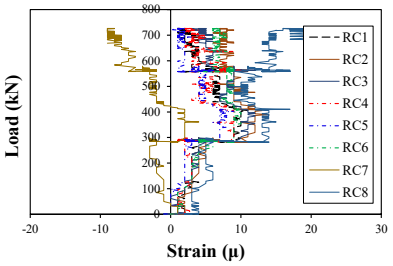

(c) Steel plate gauges

Fig. 17 Deformation of shear connector in bending test of specimen CM-550

5.4 Shear test results of finite element analysis and experiment of S-550

In Fig. 18(a), the experimental load-displacement curve of specimen S-550 is presented along with FEA results and shear strength V_n predicted by the proposed formulations. As can be seen, the elastic period is maintained until the load of 1061kN. The nominal shear strength is recorded at 1214.4kN, which is 41.45% higher than the value of specimen S-400, 715.1kN.

Regarding the estimated results, shear strengths of HVS are 1187.7kN and 1069.5kN by calculation and analysis in MIDAS, respectively. In general, ratios of difference around 10% are acceptable results. Moreover, MIDAS FEA also provides final displacement contour as shown in Fig. 19(b). Fig. 19(c) shows crack patterns at the failure of S-550. Cracks occur in the shear span. Also, diagonal cracks are simulated by open-elements in the analysis.

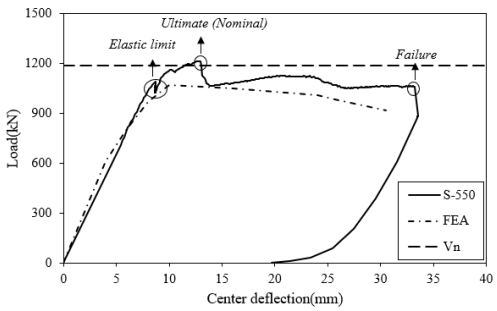

(a) Load-displacement curve of S-550

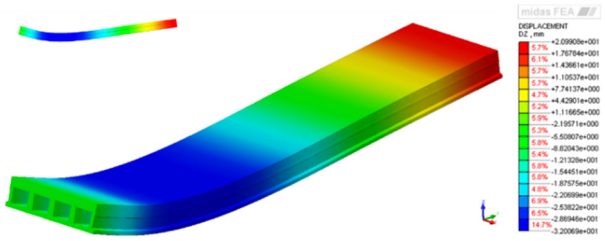

(b) Displacement contour in MIDAS FEA

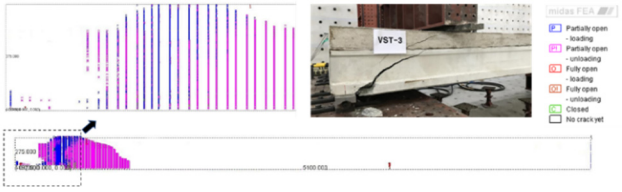

(c) Crack patterns in test and analysis of S-550

Fig. 18 Results of S-550

6. Conclusions

This study introduces newly developed rib precast prestressed concrete slabs including Hidden boundary Void Slab (HVS). Overviews of slabs such as advantages, structural details, manufacturing processes are presented. Especially, the study scrutinizes performances of light-weight slabs with bi-tensional prestressed in terms of experiments, analysis, and formulations. Overall, HVS demonstrates promising applications in the field of real prestressed precast concrete industries for construction.

Obtained assessments are highlighted as follows:

- Experimental results provide applicable data for the research and manufacture of HVS. Moreover, the characteristic of composite structures is verified:
  - With HVS, the addition of topping concrete enhances 45% bending strength and 41.45% shear strength, as well as, eliminates brittle behaviors of PC members. Although the brittle performance is usual in a fully prestressed concrete component, it should be considered carefully in designs based on its function.
  - Proposed shear connectors demonstrate effective applications when balancing different cambers between PC members but not creating structural distinguishment at adjacent areas of HVS.
  - Crack patterns reflect failure modes and structural characteristics of specimens.
- An originality in the paper is to calculate processes of flexural and shear strengths of prestressed concrete flagged sections. Simultaneously, the thickness design of specific shear connectors is provided. According to comparisons with experimental results, proposed formulations are feasible and effective with small differences.
- The finite element method by MIDAS FEA is manipulated as a predicting approach. The analysis gives acceptable conservative results in terms of flexural and shear capacity for HVS. While other behaviors such as deformations, crack patterns are suitable for real situations. In general, analysis results by MIDAS FEA are worthy to consult when predicting the actual performances.

Acknowledgments

This research is sincerely supported by IS Dongseo research project and a grant (NRF-2017R1A4A1015660) of NRF in South Korea in 2018. Sincerely we appreciate for the support.

References

AASHTO (2002), Standard Specifications for Highway Bridges, (17th edition), American Association of State Highway and Transportation Officials, Washington, DC, USA.

ACI Committee 318 (1977), Building Code Requirements for Reinforced Concrete (ACI 318-77), American Concrete Institute, Detroit, MI, USA.

ACI Committee 318 (1983), Building Code Requirements for Reinforced Concrete (ACI 318-83), American Concrete Institute, Detroit, MI, USA.

ACI Committee 318 (2011), Building code requirements for structural concrete and commentary, American Concrete Institute, Farmington Hills, MI, USA.

ACI Committee 446 (1991), "Fracture Mechanics of Concrete: Concepts, Models and Determination of Material Properties (ACI 446.1R-91) (Reapproved 1999)", American Concrete Institute, Farmington Hills, MI, USA.

ACI 318-14 (2014), Building Code Requirements for Structural Concrete and Commentary, American Concrete Institute, Farmington Hills, MI, USA.

Amadeo, B.C., Jesús, D.A. and Elena, O.S. (2018), "Seismic performance and damage evaluation of a waffle-flat plate structure with hysteretic dampers through shake-table tests", *Earthq. Eng. Struct. Dyn.*, **47**(5), 1250-1269. https://doi.org/10.1002/eqe.3016

Attila, B.B. (2014), "An Introduction to Voided Slabs, Design Considerations, and Contemporary Project Case Studies. First Edition", Concrete Reinforcing Steel Institute (CRSI).

Björn, E. (2008), *Structural connections for precast concrete buildings*, International Federation for Structural Concrete (fib).

Branson, D.E. and Kripanarayanan, K.M. (1971), "Loss of prestress, camber and deflection of non-composite and composite prestressed concrete structures", *Precast/Prestressed Concrete Inst. J.*, **16**(5), 22-52.

Chahnasir, S.E., Zandi, Y., Shariati, M., Dehghani, E., Toghroli, A., Mohamad, T.E., Shariati, A., Safa, M., Wakil, K. and Khorami, M. (2018), "Application of support vector machine with firefly algorithm for investigation of the factors affecting the shear strength of angle shear connectors", *Smart Struct. Syst., Int. J.*, **22**(4), 413-424. https://doi.org/10.12989/sss.2018.22.4.413

Churakov, A. (2014), "Biaxial hollow slab with innovative types of voids", *Constr. Unique Build. Struct.*, **6**(21), 70-88.

CSA A23.3-14 (2014), Design of concrete structures, Canadian Standards Association, Mississauga, ON, Canada.

CUR Recommendations 86 (2008), BubbleDeck Voided Flat Slab Solutions- Technical Manual & Documents, Centre for Civil Engineering Research and Codes (CUR).

DIN 1045-1:2008 (2009), *Tragwerke aus Beton, Stahlbeton und Spannbeton, Teil 2: Bemessung und Konstruktion*, Betonkalender 2009, Ernst & Sohn, Berlin, Germany, pp. 478-584.

Doan, Q.H. and Lee, D. (2017), "Optimum topology design of multi-material structures with non-spurious buckling constraints", *Adv. Eng. Software*, **114**, 110-120. https://doi.org/10.1016/j.advengsoft.2017.06.002

EN 1992-1-1 (2004), Eurocode 2 - Design of concrete structures - Part 1-1: General rules and rules for buildings, European Committee for Standardization, Brussels, Belgium.

Grandić, D., Šćulac, P. and Grandić, I.Š. (2015), "Shear resistance of reinforced concrete beams in dependence on concrete strength in compressive struts", *Technical Gazette*, **22**(4), 925-934. https://doi.org/10.17559/TV-20140708125658

Guo, Y.T., Tao, M.X., Nie, X. and Fan, J.S. (2017), "Rigidity and moment distribution of steel-concrete composite waffle floor systems considering the spatial effect", *Eng. Struct.*, **143**, 498-510. https://doi.org/10.1016/j.engstruct.2017.04.042

KCI (2012), Explanation of Concrete Structural Design Standard, Korea Concrete Institute, Korea.

Kim, T.H., Seong, D.J. and Shin, H.M. (2012), "Seismic performance assessment of hollow reinforced concrete and prestressed concrete bridge columns", *Int. J. Concrete Struct. Mater.*, **6**(3), 165-176. https://doi.org/10.1007/s40069-012-0015-y

Kuo, W.W., Hsu, T.T.C. and Hwang, S.J. (2014), "Shear strength of reinforced concrete beams", *ACI Struct. J.*, **111**(4), 809-818.

Laskar, A., Hsu, T.T.C. and Mo, Y.L. (2010), "Shear Strengths of Prestressed Concrete Beams Part 1: Experiments and Shear Design Equations", *ACI Struct. J.*, **107**(3), 330-339.

Lee, D.K. and Banh, T.T. (2018), "Multi-material topology optimization design for continuum structures with crack patterns", *Compos. Struct.*, **186**, 193-209. https://doi.org/10.1016/j.compstruct.2017.11.088

Lee, S.S. and Park, K.S. (2010), "Evaluation for Horizontal Shear Strength of Precast Concrete Slab with the Inverted Rib", *J. Archit. Inst. Korea Struct. Constr.*, **26**(1), 29-36.

Lee, D.K., Kim, D.W., Lee, J.H., Noh, P.S. and Park, S.S. (2015), "Analytical testing and evaluation of truss typed structures for tunnel maintenance", *Smart Struct. Syst.*, *Int. J.*, **15**(4), 949-961. https://doi.org/10.12989/sss.2015.15.4.949

Lee, D.K., Shin, S.M. and Doan Q.H. (2018), "Real-time robust assessment of angles and positions of nonscaled steel outrigger structure with Maxwell-Mohr method", *Constr. Build. Mater.*, **186**, 1161-1176. https://doi.org/10.1016/j.conbuildmat.2018.07.212

Lesani, M., Bahaari, M.R. and Shokrieh, M.M. (2017), "Response to the discussion on von-Mises stress attenuation along crown line of CHS T-joints", *J. Constr. Steel Res.*, **137**, 372-374. https://doi.org/10.1016/j.jcsr.2015.01.022

Li, X.H., Wu, G., Popal, M.S. and Jiang, J. (2018a), "Experimental and numerical study of hollow core slabs strengthened with mounted steel bars and prestressed steel wire ropes", *Constr. Build. Mater.*, **188**, 456-469. https://doi.org/10.1016/j.conbuildmat.2018.08.073

Li, Y.A., Hsu, T.T. and Hwang, S.J. (2018b), "Shear strength of prestressed and nonprestressed concrete beams", *Concrete Int.*, **39**(9), 53-57.

Major, Z. (2012), "Applicability of displacement controlled fatigue test methods for compliant structures", *IMEKO TC15 – Experimental Mechanics – Proceedings of 11th Youth Symposium on Experimental Solid Mechanics*, Brasov, Romania, May-June.

Marais, C.C., Robberts, J.M. and van Rensburg, B.W.J. (2010), "Spherical void formers in concrete slabs", *J. South Afr. Inst. Civil Eng.*, **52**(2), 2-11.

Mattock, A.H. (1984), "Modification of ACT Code Equation for Stress in Bonded Prestressed Reinforcement at Flexural Ultimate", *ACI J.*, **81**(4), 331-339.

McCormac, J.C. and Brown, R.H. (2015), *Design of Reinforced Concrete*, (10th Edition), Clemson University, SC, USA.

McGregor, J.G. (1984), Special Study for the Canadian Code, Private Communication.

MacGregor, J.G., Wight, J.K., Teng, S. and Irawan, P. (1997), *Reinforced Concrete*: *Mechanics and Design*, (3rd Edition), Prentice-Hall, Upper Saddle River, NJ, USA.

Motezaker, M. and Eyvazian, A. (2020a), "Post-buckling analysis of Mindlin Cut out-plate reinforced by FG-CNTs", *Steel Compos. Struct.*, *Int. J.*, **34**(2), 289-297. https://doi.org/10.12989/scs.2020.34.2.289

Motezaker, M. and Eyvazian, A. (2020b), "Buckling load optimization of beam reinforced by nanoparticles", *Struct. Eng. Mech.*, *Int. J.*, **73**(5), 481-486. https://doi.org/10.12989/SEM.2020.73.5.481

Motezaker, M. and Kolahchi, R. (2017), "Seismic response of concrete columns with nanofiber reinforced polymer layer", *Comput. Concrete*, *Int. J.*, **20**(3), 361-368. https://doi.org/10.12989/CAC.2017.20.3.361

Nguyen, T.N.H., Tan, K.H. and Kanda, T. (2019), "Investigations on web-shear behavior of deep precast, prestressed concrete hollow core slabs", *Eng. Struct.*, **183**, 579-593. https://doi.org/10.1016/j.engstruct.2018.12.052

Paik, I.K. and Na, S.G. (2018), "Evaluation of Noise Insulation Performance for Void Deck Slab System which Combines Deck Plates with a Voided Slab System", *Int. J. Appl. Eng. Res.*, **13**(10), 7348-7359.

Park, H.J., Kim, M.K., Hwang, D.K., Hwang, H.S. and Kim, H.S. (2009), "Vibration Performance Evaluation of Two-Way Hollow Slab with Walking Load", *J. Earthq. Eng. Soc. Korea*, **13**(5), 11-21.

Pavlina, E. and Van Tyne, C.J. (2008), "Correlation of yield strength and tensile strength with hardness for steels", *J. Mater. Eng. Perform.*, **17**(6), 888-893. https://doi.org/10.1007/s11665-008-9225-5

PCI (2004), PCI Design Handbook-Precast and Prestressed Concrete, (6th edition), Precast/Prestressed Concrete Institute, Chicago, IL, USA.

Ritter, W. (1899), "Die Bauweise Hennebique", (The Hennebique system), Schweizerische Bauzeitung, Bd. XXXIII, No. 7, January 1899.

Sedghi, Y., Zandi, Y., Shariati, M., Ahmadi, E., Azar, V.M., Toghroli, A., Safa, M., Mohamad, T.E., Khorami, M., Wakil, K. and Khorami, M. (2018), "Application of ANFIS technique on performance of C and L shaped angle shear connectors", *Smart Struct. Syst.*, *Int. J.*, **22**(3), 335-340. https://doi.org/10.12989/sss.2018.22.3.335

Shetkarand, A. and Hanche, N. (2015), "An experimental study on bubble deck slab system with elliptical balls", *Indian J. Sci. Res.*, **12**(1), 21-27.

Sovják, R., Havlásek, P. and Vítekc, J. (2012), "Long-term behavior of concrete slabs prestressed with CFRP rebars subjected to four-point bending", *Constr. Build. Mater.*, **188**, 781-792. https://doi.org/10.1016/j.conbuildmat.2018.08.084

Thorenfeldt, E., Tomaszewicz, A. and Jensen, J.J. (1987), "Mechanical Properties of High-strength Concrete and Application in Design", *Proceedings of the Symposium Utilization of High-Strength Concrete*, Trondheim, Norway, pp. 149-159.

Tureyen, A.K. and Frosch, R.J. (2003), "Concrete shear strength: Another perspective", *ACI Struct. J.*, **100**(5), pp. 609-615.

Wu, Y. and Peng, K. (2018), "Finite Element-Smeared Crack Combined Algorithm based Bridge Corbel Analysis", *IOP Conference Series*: *Earth and Environmental Science*, **189**(2), p. 022017. https://doi.org/10.1088/1755-1315/189/2/022017

Yang, K.H., Lee, Y.J. and Joo, D.B. (2016), "Flexural behavior of post-tensioned lightweight concrete continuous one-way slabs", *Int. J. Concrete Struct. Mater.*, **10**(4), 425-434. https://doi.org/10.1007/s40069-016-0169-0

Zuo, Y., Qian, Z., Garboczi, E.J. and Ye, G. (2010), "Numerical simulation of the initial particle parking structure of cement/geopolymer paste and the dissolution of amorphous silica using real-shape particles", *Constr. Build. Mater.*, **185**, 206-219. https://doi.org/10.1016/j.conbuildmat.2018.07.063

CC

Appendix: Theoretical Backgrounds and Proposed Calculations

This Appendix aims to clarify the proposed predictions shown in Sections 2 and 3.

A. Shear connector design

First, the slab is cambered with a deflection δ in the middle, due to the prestressed tendons. According to Appendix B in the report of Branson and Kripanarayanan (1971), this phenomenon is similar to the case that a uniformly distributed load impacts to slab. Therefore, assume that there is a uniformly distributed load ω resulting in deflection δ at the middle of the slab, as shown in Eq. (A1)

$$\delta = \frac{5\omega L^4}{384EI} \Rightarrow \omega = \frac{384EI}{5L^4}\delta \quad \text{(A1)}$$

where

δ = deflection at the middle of the slab, equal to 20mm for designing (according to real records)
L = length of the slab
EI = stiffness of the slab

Shear connectors are placed at 1/4 of total length of the members from two ends. Therefore, at each connector, there is another deflection δ_x. In practice, when balancing difference camber between two PC members, a force P_u impacts on slab through the shear connector.

The deflection δ_x and the force P_u are calculated as follow

$$\delta_x = \frac{\omega x}{24EI}(L^3 - 2Lx^2 + x^3)$$
$$P_u = \frac{48EI\delta_x}{L^3} \quad \text{(A2)}$$

where, x = 1/4 of the total length of the slab.

The shear connectors also suffer the load P_u, so it is required that steel plates and U-bolt have to be ensured during the assembly. The shape of steel plates has to be appropriate with geometries of slabs and convenient for assembling. While the thicknesses of both steel plates and U-bolts needs to be designed to satisfy the structural performance.

B. Nominal moment capacity

More recently, Eq. (B1), considering various factors such as the reinforcing index, the partial prestressing ratio, concrete strength, prestressing and reinforcing steel grades and the different amount of the compression reinforcement, was proposed by Mattock (1984) and adopted in ACI Code in 1983. This equation is still used for the latest revision of ACI 318 in 2014 as well as adopted in other local standards as PCI 2004, KCI 2012.

$$f_{ps} = f_{pu}\left(1 - \frac{\gamma_p}{\beta_1}\left\{\rho_p \frac{f_{pu}}{f_c^{'}} + \frac{d}{d_p}(\omega - \omega^{'})\right\}\right) \quad \text{(B1)}$$

in which

γ_p = coefficient related to yielding ratio. The value is 0.55; 0.4 and 0.28 when $f_{py}/f_{pu} \geq 0.80$; 0.85 and 0.90, respectively.

f_{py} = yielding strength of prestressed strands,

β_1 = coefficient related to the equivalent rectangular stress block. The value is 0.85 when $f_c^{'} < 28$ MPa and equal to $0.85 - 0.007(f_c^{'} - 28) \geq 0.65$,

$\omega = \frac{A_s f_y}{bdf_c^{'}}$ and $\omega^{'} = \frac{A_s^{'} f_y}{bdf_c^{'}}$ are reinforcing index,

$A_s, A_s^{'}$= area of tension and compression reinforcement, respectively,

d_p = distance from extreme compression fibers to the centroid of the prestressing reinforcement.

If a compression reinforcement is to be considered in Eq. (B1), the parameter $\rho_p f_{pu}/f_c^{'} + d/d_p(\omega - \omega^{'})$ should not be taken less than 0.17, and the distance $d_s^{'}$ between the top concrete fiber and the center of compression steel should not exceed $0.15d_p$. However, the effect of sectional shapes is not considered, because the section which has the flange such as I-type section or T-type section is treated as a rectangular section.

In Canadian Code-CSA, McGregor (1984) suggested the following equation to compute f_{ps}

$$f_{ps} = f_{pu}\left(1 - K_p \frac{c}{d_p}\right) \quad \text{(B2)}$$

where

$K_p = 3\left(1 - \frac{f_{py}}{f_{pu}}\right)$ in the first proposal or $K_p = 2\left(1.04 - \frac{f_{py}}{f_{pu}}\right)$ in version CSA A23.3-14.

$c =$ neutral axis depth calculated by assuming a stress f_{pu}, in the tendons and f_y, in the non-prestressed reinforcement. Nevertheless, at this time, c is computed using the equation of force equilibrium in the section, that is, for a rectangular section:

$$0.85f_c^{'}b\beta_1 c = A_p f_{pu} + A_s f_y - A_s^{'} f_y^{'}.$$

To determine the contribution of compression flange overhangs, AASHTO Standard Specifications (2002) provide Eq. (B3) for prestressed strand stress f_{ps} of the T-section member. Eq. (B3) describes the internal equilibrium of the compressive force in the concrete and tensile force in the pre-stressed steel.

$$A_{ps}f_{ps} = (0.85f_c^{'})(\beta_1 c)b_w + (0.85f_c^{'})h_f(b - b_w) \quad \text{(B3)}$$

in which

b_w = web width
h_f = compression flange depth

A contribution of the top flange overhangs to the total internal compressive force in Eq. (B3) is $0.85f_c^{'}(b - b_w)h_f$.

In this study, to simplify calculations of flexural behaviors, the PC unit of HVS without topping concrete is

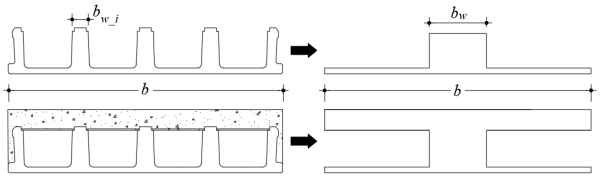

Fig. 19 Sectional-assumptions

given as an inverted-T-section member. HVS having topping concrete is given as an I-section member. Thus, the parameter b - a width of compression face - is accounted as the width of the slab, while the parameter b_w - a web width - is accounted as the total width of ribs, as shown in Fig. 19.

However, this assumption could be conflicted with the calculation of a single T-section member in terms of an effective width b_{eff}. Parameter b_{eff} is a width that is stressed uniformly to give the same compression force actually developed in a compression zone of width b. McCormac and Brown (2015) present the estimation of b_{eff} as follows.

$$b_{eff} \le \begin{cases} L/4 \\ 16h_f + b_w \\ b \end{cases} \tag{B4}$$

with L = length of slab.

This width-limitation leads to underestimate flange effects of HVS, when they are considered as sections with only one rib. Therefore, to deal with this incompatibility, b_{eff} in this thesis is accounted as a total effective width of each rib b_e, as shown in Fig. 9 of prediction procedures for the nominal flexural strength.

In order to improve the accuracy of the predicted sectional response from several existing standards, the inclusions of sectional shape, prestressed reinforcement, tensile, compressive reinforcement and concrete strength are reflected in proposed Eq. (B5). Clearly, there is some correlation among Eqs. (B1), (B2), (B3) of different standards. According to the definition of c, a new relationship between the neutral axis location and reinforcing index can be derived from the force equilibrium.

$$f_{ps} = f_{pu}\left(1 - K_p\frac{c}{d_u}\right) \tag{B5}$$

where

$$K_p = 2\left(1.04 - \frac{f_{py}}{f_{pu}}\right); \qquad d_u = \frac{A_p f_{pu} d_p + A_s f_y d_s}{A_p f_{pu} + A_s f_y}$$

For $\beta_1 c \le h_f$, then rectangular section behavior occurs

$$c = \frac{A_p f_{pu} + A_s f_y - A_s' f_y}{0.85\beta_1 f_c' b_{eff} + K_p\frac{A_p f_{pu}}{d_u}}$$

For $\beta_1 c \ge h_f$, then T-section behavior occurs

$$c = \frac{A_p f_{pu} + A_s f_y - A_s' f_y - T_f}{0.85\beta_1 f_c' b_w + K_p\frac{A_p f_{pu}}{d_u}}$$

where

$T_f = 0.85 f_c'(b_{eff} - b_w)h_f$, in the absence of topping concrete.

$T_f = 0.85 f_{ct}'(b_{eff} - b_w)h_t + 0.85 f_c'(b_{eff} - b_w)h_f$, in the presence of topping concrete taking compression strength f_{ct}' and thickness h_t.

For calculating nominal moment capacity M_n,

when $\beta_1 c \le h_f$, then the rectangular section behavior occurs

$$M_n = A_p f_{ps}\left(d_p - \frac{\beta_1 c}{2}\right) + A_s f_y\left(d_s - \frac{\beta_1 c}{2}\right) - A_s' f_y\left(d_s' - \frac{\beta_1 c}{2}\right) \tag{B6}$$

when $\beta_1 c \ge h_f$, then T-section behavior occurs

$$M_n = \left(A_p f_{ps} + A_s f_y - T_f\right)\left(d_u - \frac{\beta_1 c}{2}\right) + T_f\left(d_u - \frac{h_f}{2}\right) - A_s' f_y\left(d_s' - \frac{\beta_1 c}{2}\right) \tag{B7}$$

Note that, before Eq. (B6) or (B7) is conducted, check if the section is under-reinforced. In case of over-reinforced, the nominal moment has to be applied by other equations. Using the ACI code (2011), the reinforcing index $\bar{\omega}$ for under-reinforced section could be expressed as follows: $\bar{\omega} = 0.85\beta_1\frac{c}{d_e} \le 0.36\beta_1$, where

$$d_e = \frac{A_p f_{pu} d_p + A_s f_y d_s}{A_p f_{ps} + A_s f_y}$$

Note that this calculation step could be omitted since d_e is very close to d_u. Therefore, in this study:

$\frac{c}{d_u} \le 0.42$, the section is under-reinforced

$\frac{c}{d_u} > 0.42$, the section is over-reinforced.

The procedure of proposed calculations is summarized in Fig. 9. To validate the calculation with experiment data, the ultimate load P_u in four-point bending test is calculated by: $P_u = 2\frac{M_n}{l_p} -$ Self-weight,

in which: l_p = distance from loading points to simply-supports. Self-weight is measured directly at the factory.

C. Shear strength

Most of the design methods superimpose the shear resistance of the concrete, V_c, due to an aggregate interlock, a shear transfer in the compression zone, and a dowel action with the shear resistance provided by the stirrups, V_s, and the shear resistance provided by the vertical component of the force in the draped prestressing strand, V_p, to determine the shear capacity, V_n, of the section

$$V_n = \left(V_s + V_c + V_p\right) \quad or \quad V_n = (V_s + V_c), \text{ due to } V_p \text{ is included in } V_c \tag{C1}$$

Shear strength provided by shear reinforcement V_s

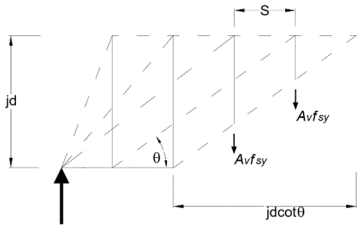

Fig. 20 Stirrup contribution to shear capacity

Recently, a truss model by MacGregor *et al*. (1997) is the basis for the stirrup contribution to shear capacity for the shear methods. This model represents the load paths in cracked concrete as a truss with the stirrups acting as the vertical tension members, the concrete acting as the compression chord and the compression diagonals, and the flexural reinforcement acting as the tension chord. An example of a truss model for a reinforced concrete beam is shown in Fig. 20.

As the model,

$A_v f_{sy}$ = stirrup forces, with
A_v = the area of shear reinforcement within spacing s
f_{sy} = specified yield strength of transverse reinforcement
θ = angle of the inclined struts.

Obtaining the stirrup forces, $A_v f_{sy}$, the truss in this figure becomes statically determinate. In this model, the beam is proportioned so that the stirrups yield before the concrete crushes, and sufficient longitudinal steel is provided for a horizontal equilibrium. The shear resistance of the model is entirely dependent upon the amount and distribution of a transverse reinforcement. The stirrup contribution to the shear capacity is given by the equation: $V_s = \frac{A_v f_{sy}(jd\cot\theta)}{s}$.

Nowadays, when vertical shear reinforcements are ubiquitous, this kind of model is used in many countries. That is because of its advantages: clear, simple mechanical concept and easy calculation. Indeed, the provisions in various standards present implicitly to define for stirrup contribution to shear capacity.

In ACI 318 (2014), AASHTO (2002), Eurocode (EN 1991) the stirrup contribution to shear capacity is based on a truss model assuming a 45° crack pattern. With the angle of inclination conservatively set to 45°, the horizontal projection of the crack is taken as d, which is the distance from the extreme compression fiber to the centroid of the tension steel. With these assumptions

$$V_s = \frac{A_v f_{sy} d}{s} \quad \text{(ACI 318 2014, AASHTO 2002)}$$
$$\text{or} \quad V_s = \frac{A_v f_{sy}(0.9d)}{s} \quad \text{(EC2 1991)} \qquad \text{(C2)}$$

However, this assumption is conservative for prestressed members, because the effect of prestressing causes diagonal cracking to form at a shallower angle, thus intercepting more stirrups than predicted by the 45° truss model. Therefore, several codes consider diverse methods for the variable-angle of the inclined struts, θ, as shown in Eq. (C3)

$$V_s = \frac{A_v f_{sy} d\cot\theta}{s}, \quad \theta \text{ is given as a function of } \varepsilon_x$$
(AASHTO LRFD 2002)
$$V_s = \frac{A_v f_{sy} d\cot\theta}{s}, \quad \theta = 29 + 7000\varepsilon_x$$
(CSA 2014)
$$V_s = \frac{A_v f_{sy}(0.9d)\cot\theta}{s}, \quad 1 \le \cot\theta \le 2.5$$
(EN 2004) (C3)

Besides, when there are not enough parameters to calculate θ, Grandíc *et al*. (2015) provides the compilation of approximate values just based on the compressive strength of concrete. The compilation is obtained from EN (2004), DIN (2009) and CSA (2014) approaches. In this thesis, θ = 37° is applied for $f_c' = 45$ MPa, and θ = 40° is applied for $f_c' = 40$ MPa.

Moreover, in cases of using the inclined stirrup as HVS in this study, another suitable one is scrutinized. Ritter (1899) suggested first the truss model, Ritter model, of parallel chords for a calculation of shear strength of the beam with a web reinforcement. The calculation principle of the truss model is shown in Fig. 21. It is assumed that all the bars of the truss are jointed with hinges, the compression zone of concrete on the top part and the longitudinal tensile reinforcement of the beam are considered respectively as the upper and lower chords, and the internal level arm is the vertical distance between both chords. The stirrups and bent-up reinforcements are considered as the tensed web bars with inclination α. The concrete on the web is considered as the compressed web bars with an inclination θ.

When the internal force in the web reinforcement is calculated, an inclined section (ab) is assumed to be parallel with the compressed web bar of concrete, so the total tensile force (T) of the web reinforcements intersected acts only on the section and the vertical component is in equilibrium with the reaction at the support.

Consequently, the angle between the inclined section and normal plane of the web reinforcement is

$$\beta = \theta + \alpha - 90^{\circ} \qquad \text{(a)}$$

and the action length of the web reinforcements is

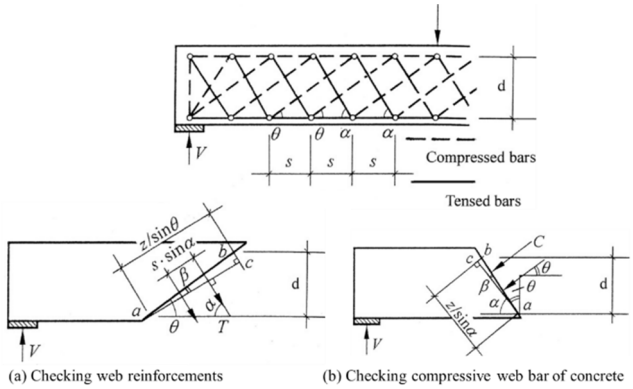

Fig. 21 Mechanical model of Ritter model

$$\bar{a}\bar{c} = \frac{d}{\sin\theta}\cos\beta = d\frac{\sin(\alpha+\theta)}{\sin\theta} \quad \text{(b)}$$

so the total tensile force of the web reinforcements on the section is

$$T = \frac{A_{sv}f_{yv}}{s.\sin\alpha} \times d\frac{\sin(\alpha+\theta)}{\sin\theta} = \frac{A_{sv}f_{yv}d}{s}(\cot\alpha + \cot\theta) \quad \text{(c)}$$

In general, the equilibrium condition of vertical forces according to Fig. 21 is established

$$V_s = T\sin\alpha = \frac{A_{sv}f_{yv}d}{s}\sin\alpha\,(\cot\alpha + \cot\theta) \quad \text{(C4)}$$

Note that the parameter d used from Eqs. (C1) to (C4) will be replaced by h_{sv} in order to avoid the duplication with other equations.

Shear strength provided by concrete V_c

The concrete contribution is a function of the type of shear cracking that controls (flexure-shear or web-shear) at a given cross-section. Flexure-shear cracking controls where a moment is large and shear exists, and web-shear cracking typically controls in thin web members near the supports where a moment is small and shear is large. The contribution of prestressing to shear resistance is included in the equations for the concrete contribution.

A flexure-shear crack originates as a vertical flexural crack in a member. As the crack penetrates deeper into the cross-section, it becomes inclined as a result of the shear stresses within the section. Shear capacity controlled by the flexure-shear cracking is the sum of the shear required to initiate flexural cracking plus an increment necessary to extend the crack to a flexure-shear crack. The flexure-shear cracking capacity of prestressed concrete is given in ACI 318 (1977), AASHTO (2002), KCI (2012) by the following equations

$$\begin{aligned} &V_{ci} = 0.6\sqrt{f_c'}b_w d + V_d + \frac{V_i M_{cr}}{M_{max}} \geq 1.7\sqrt{f_c'}b_w d \\ &(\text{ACI 318 1977, AASHTO 2002}) \\ &V_{ci} = 0.05\lambda\sqrt{f_c'}b_w d_p + V_d + \frac{V_i M_{cr}}{M_{max}} \geq 0.17\lambda\sqrt{f_c'}b_w d \\ &(\text{KCI 2012}) \end{aligned} \quad \text{(C5)}$$

Note that, KCI 2012 uses units (MPa, mm), the others use units (psi, in).

where

λ = lightweight concrete coefficient

V_d = shear force at section due to unfactored dead load (self-weight and superimposed).

M_{max} = maximum factored moment at section due to externally applied loads

V_i = shear force occurring simultaneously with M_{max}

M_{cr} = moment causing flexural cracking at the cross-section due to externally applied loads and is given in the code as $M_{cr} = \frac{I_{gc}}{y_{tc}}\left(6\sqrt{f_c'} + f_{pe} - f_d\right)$.

In this equation

I = gross moment of inertia of the composite cross-section

y_{tc} = distance from centroidal axis of the gross composite section to the extreme tension fiber

f_{pe} = compressive stress in the concrete due to the effective prestressing force at the extreme tension fiber of the cross-section.

f_d = tensile stress due to the unfactored dead load at the extreme tension fiber of the cross-section.

The other types of shear failures considered in the design of prestressed concrete members produce the result of web-shear cracking. Web-shear cracks form, when the principal tensile stresses from shear exceed the tensile strength of the concrete. The resistance to web-shear cracking is due to the tensile strength of the concrete and the compressive forces in the section due to the prestressing force and the applied loads. In addition, the vertical component of the prestressing force due to draped strands provides resistance to the shear. The expression for web-shear strength usually governs for heavily prestressed beams with thin webs, especially when the beam is subject to large concentrated loads near the supports.

The web-shear equation predicts the shear strength at the onset of web-shear cracking and is given in the ACI 318, AASHTO 2002, KCI 2012 as

$$\begin{aligned} &V_{cw} = \left(3.5\sqrt{f_c'} + 0.3f_{pc}\right)b_w d + V_p \\ &(\text{ACI318 2014, AASHTO 2002}) \\ &V_{cw} = \left(0.29\lambda\sqrt{f_c'} + 0.3f_{pc}\right)b_w d_p + V_p \\ &(\text{KCI 2012}) \end{aligned} \quad \text{(C6)}$$

The contribution of the concrete to shear strength, V_c, is lesser than those of V_{ci} and V_{cw}. However, the calculation of V_c in these design methodologies are commented to be confused and difficult for engineers, since multiple equations are used.

This study proposes unified design provisions for calculating the shear strength of prestressed concrete members. The design methodology is the unification of three concepts.

- Compression zone concept (V_c is proportional to $\sqrt{f_c'}b_w c$): This concept was suggested by Tureyen and Frosch (2003) and verified by Kuo *et al*. (2014). The essence of this concept is that the contribution of concrete V_c is proportional to the depth of the uncracked compression zone c.
- Arch action concept (V_c is proportional to $\left(\frac{V_u d}{M_u}\right)^{0.7}$): This concept states that the contribution of concrete V_c is also proportional to the shear span-depth ratio to the power of 0.7.
- Size effect concept (V_c is proportional to $\frac{1}{\sqrt{1+h/h_0}}$). This concept was adopted from a report by Joint ACI-ASCE Committee 446, Fracture Mechanics of

Concrete, prepared under the chairmanship of Zdeněk Bažant (1999). It states that V_c is related to a size factor which is a function of the sectional height h.

By incorporated two factors including compression zone concept and arch action concept, Laskar *et al*. (2010) proposed a simple and accurate shear strength equation, called UH methods. The UH method was verified with comparisons with ACI and AASHTO Provisions. Then it was developed for I-section beam by Li *et al*. (2018a, b) after combining these three concepts, as the following equations

$$V_c = 17\lambda\left(\frac{V_u d}{M_u}\right)^{0.7}\sqrt{f_c'}b_w c\frac{1}{\sqrt{1+\frac{h}{11.8}}}F_p F_{flange} \leq 10\lambda\sqrt{f_c'}b_w c F_p F_{flange} \quad \text{(C7)}$$

Note that,the units here (psi, in).

where

$$c = d\left(\sqrt{(\rho n)^2 + 2\rho n} - \rho n\right) \text{ with } \rho = \frac{A_s + A_p}{b_w d} \text{ and } n = \frac{E_s}{E_c}.$$

$$F_p = \sqrt{1 + \frac{P_e}{0.33\lambda\sqrt{f_c'}b_w d}} \text{ with } P_e = A_p f_{pe}$$

$$F_{flange} = 1.2 \text{ for } \mathrm{I-section\ only}$$

Eq. (C7) is inherited but with an adjustment and transformation in order to be compatible with two concepts of slabs in this study. The proposed equation is shown in Eq. (C8).

$$V_c = 1.42\lambda\left(\frac{d_u(\ell - 2x)}{x(\ell - x)}\right)^{0.7}\sqrt{f_c'}b_w c\frac{1}{\sqrt{1+\frac{h}{300}}} \times F_p F_{flange} + V_p \leq 0.83\lambda\sqrt{f_c'}b_w c F_p F_{flange} \quad \text{(C8)}$$

Note that, the units here (MPa, mm).

where $\frac{V_u d}{M_u}$ in arch action concept is not available in the predicting task, so according to ACI-318 it can be expressed as $\frac{\ell - 2x}{x(\ell - x)}$, with ℓ is the span length and x is the distance from the section being investigated to the support.

Here, the parameter d or d_p used in Eq. (C7) is replaced by d_u.

d_u is the distance from extreme compression fibers to the general centroid of all tensile reinforcements, in cases of partly prestressed members. d_u is taken from Eq. (B7)

$$d_u = \frac{A_p f_{pu} d_p + A_s f_y d_s}{A_p f_{pu} + A_s f_y}.$$